

Emergence of Multiscale Dynamics in Colloidal Gels

Jae Hyung Cho,¹ Roberto Cerbino,² and Irmgard Bischofberger¹

¹*Department of Mechanical Engineering, Massachusetts Institute of Technology, Cambridge, Massachusetts 02139, USA*

²*Dipartimento di Biotecnologie Mediche e Medicina Traslazionale, Università degli Studi di Milano, Via. F.lli Cervi 93, Segrate (MI) I-20090, Italy*

(Dated: January 27, 2023)

To gain insight into the kinetics of colloidal gel evolution at low particle volume fractions ϕ , we utilize differential dynamic microscopy to investigate particle aggregation, geometric percolation, and the subsequent transition to nonergodic dynamics. We report the emergence of unexpectedly rich multiscale dynamics upon the onset of nonergodicity, which separates the wave vectors q into three different regimes. In the high- q domain, the gel exhibits ϕ -independent internal vibrations of fractal clusters. The intermediate- q domain is dominated by density fluctuations at the length scale of the clusters, as evidenced by q -independence of the relaxation time τ . In the low- q domain, the scaling of τ as q^{-3} suggests that the network appears homogeneous. The transitions between these three regimes introduce two characteristic length scales, distinct from the cluster size.

Rich rheological behavior of colloidal gels arises from the coexistence of multiple length and time scales that characterize their structure and dynamics. Colloidal gels with low particle volume fractions ϕ form space-spanning networks of fractal clusters through particle aggregation or phase separation [1–5]. The self-similarity of these fractal aggregates originates in a broad range of length scales that constitute the gels from the size of individual particles to that of clusters. In addition, the kinetic arrest during gelation prevents the systems from ever reaching equilibrium states [6–8]. The nonequilibrium gels constantly evolve via structural rearrangements triggered by thermal agitation and residual stresses, even in the absence of external perturbations [9–12]. The ceaseless change in structure, in turn, leads to a continuous evolution of the dynamics.

Understanding the microscopic behavior of colloidal gels, therefore, necessitates both spatially and temporally comprehensive investigation, which poses several challenges to experimentalists. The dynamics of gel networks has been extensively studied with various scattering techniques, such as dynamic light scattering [13–17], diffusing wave spectroscopy [18–22], and X-ray photon correlation spectroscopy [23, 24]. Their applications to the characterization of evolving gels, however, have been limited by small ranges of accessible length scales and prolonged data acquisition during which the systems significantly age. This lack of extensivity in experimental characterization has prevented a coherent description of the dynamics of colloidal gels.

In this Letter, we trace the entire kinetic pathway, from stable suspensions through aged gels, of colloidal gelation and network evolution over large ranges of length and time scales using differential dynamic microscopy (DDM) [25, 26]. The motion of particles and their aggregates initially slows down through two consecutive stages, while the system remains ergodic. As the gel evolves, network fluctuations become greatly suppressed, leading to the onset of nonergodicity. Three dynamically distinct

ranges of length scales, or wave vectors q , then emerge, unveiling structural hierarchy and bulk elasticity of the gel. In the high- q domain, corresponding to length scales considerably smaller than the size of the largest aggregate units, or clusters, the network behaves as internally vibrating fractals. In the intermediate- q domain, the dynamics is dominated by the collective motion over the scale of the clusters. In the low- q domain, the gel fluctuates as a homogeneous elastic network within a viscous solvent. The transitions between these three regimes are determined by both the structure and the elasticity of the network, giving rise to two characteristic length scales. This multiscale dynamics comprehensively describes colloidal gels from the scale of fractal aggregates to that of a viscoelastic continuum, allowing us to estimate the macroscopic shear modulus in the latter two regimes.

This panoramic exploration of the gels throughout their evolution is enabled by DDM that, through optical microscopy, extracts information about the density fluctuations of a sample as in scattering techniques [25]. DDM is less susceptible to the effects of multiple scattering that render the use of traditional far-field scattering techniques impracticable [27]. Moreover, simultaneous access to ensemble-averaged information at several hundreds of q over more than two decades ($q = 0.05 - 10 \mu\text{m}^{-1}$) allows comprehensive characterization of the evolving samples. We use a CMOS camera (Prime Mono, 2048×2048 pixels, Photometrics) mounted on an inverted microscope (Eclipse TE2000-U, Nikon) with two objectives of magnifications $M = 20\times/60\times$, and numerical apertures $\text{NA} = 0.50/1.20$ (water immersion), respectively. The samples are loaded in rectangular glass capillary tubes (Vitrocom) of thickness 100 μm . We repeat some of our experiments with thicker tubes of 200 μm and 300 μm to check the reproducibility of the results, and confirm no influence of the finite thickness. For the computation of $f(q, \Delta t)$, we use 1000 frames acquired at frame rates from 5 fps through 100 fps.

We utilize polystyrene-poly(N-isopropylacrylamide)

(PS-PNIPAM) core-shell colloidal particles synthesized by emulsion polymerization based on the protocol of Ref. [22, 28]. The details of the synthesis are described in the Supplemental Material [29]. The resulting thermosensitive PNIPAM shell covering the PS core induces a long-ranged steric repulsion that stabilizes the system below the gelation temperature $T_g \approx 25^\circ\text{C}$. With increasing temperature, the shell shrinks, reducing the range of the repulsion, which causes aggregation of the particles by van der Waals attraction. Hence, we can precisely control the initiation of the gelation from a fully stable suspension simply by adjusting the system temperature T . To minimize the effect of electrostatic interactions and sedimentation, we add 0.5M of sodium thiocyanate (NaSCN) to screen the charges, and density-match the system using a $\text{H}_2\text{O}/\text{D}_2\text{O}$ mixture of 52/48 v/v. The hydrodynamic radius a of the particles measured via dynamic light scattering (BI-200SM, Brookhaven Instruments) is 116.3 ± 1.8 nm at 30°C .

We initiate the gelation of a system at $\phi = 0.8\%$ by a sudden temperature increase from 20°C to 30°C at $t = 0$ s. To quantify the dynamics at different t in the micrographs as the ones shown in Fig. 1(a-c), we focus on the fast dynamics of colloidal gels due to thermal fluctuations [14], by assuming the following form of the

normalized intermediate scattering function

$$f(q, \Delta t) = (1 - C(q)) \exp \left[- \left(\frac{\Delta t}{\tau(q)} \right)^{p(q)} \right] + C(q), \quad (1)$$

which represents a stretched exponential decay from one to the nonergodicity parameter $C(q)$. Here, Δt denotes the delay time, $\tau(q)$ the relaxation time, and $p(q)$ the stretching exponent. Because of the rather complex form of Eq. (1), the domain of Δt must be carefully defined to ensure satisfactory quality of the fits. The details of the fitting procedures are delineated in the Supplemental Material [29].

In the first stage until $t \approx 400$ s, the particles form aggregates, as seen in the micrograph of Fig. 1(a). The temporal change of the relaxation time $\tau(q)$ at $q = 4.0 \mu\text{m}^{-1}$ or $qa = 0.47$, shown in Fig. 1(d), exhibits a power law with an exponent 0.61; this growth rate is similar to that of diffusion-limited cluster aggregation (DLCA) [1, 2]. In DLCA, the mean hydrodynamic radius R_h of aggregates scales as $t^{1/d_f} = t^{0.57}$ with the fractal dimension $d_f = 1.75$ [2, 30, 31]. Using $\tau = 1/(Dq^2)$, where D is the diffusion coefficient of the aggregates, and the Stokes-Einstein relation $D = k_B T / (6\pi\eta R_h)$, where k_B is the Boltzmann constant and η the solvent viscosity [32], we can indeed infer that $\tau(t)$ obeys the same power law as $R_h(t)$. Moreover, from the static structure factor $S(q)$ that we calculate based on the squared modulus of Fourier-transformed images [27, 33], we find that d_f of the aggregates is 1.8 [4, 29], independent of t , also in close agreement with $d_f = 1.75$ in DLCA. Although the two relations involving D strictly apply to suspensions of monodisperse particles, while our system displays a substantial degree of polydispersity as evidenced by the value of the stretching exponent $p \approx 0.81 - 0.95$ [32] and even more clearly by the images, the power law exponent of $\tau(t)$ stays nearly independent of q , confirming the resemblance of the aggregation to DLCA.

The second stage of evolution ($400 \text{ s} < t < 2000 \text{ s}$) in Fig. 1(d) displays a steeper power law of $\tau(t)$ with an exponent 1.16, while $p(t)$ monotonically decreases to ~ 0.6 . We suggest that the transition of the dynamics to this second stage is induced by the geometric percolation of the clusters. As the percolation starts to constrain the displacements of the clusters, a marked slowdown of their motion ensues. This scenario is consistent with the observed decrease in p with t to $p \approx 0.6$ at late times, which indicates a widening distribution of relaxation times that accompanies the slowdown. The stretched exponential relaxation of colloidal gels is generally understood as the superposition of the multiple normal modes subject to overdamped dynamics, each exhibiting a single exponential decay [14]. In this framework, the distribution of characteristic time scales of the exponentials broadens as p decreases from 1 to approximately 0.65, where the probability density function bears the largest full width

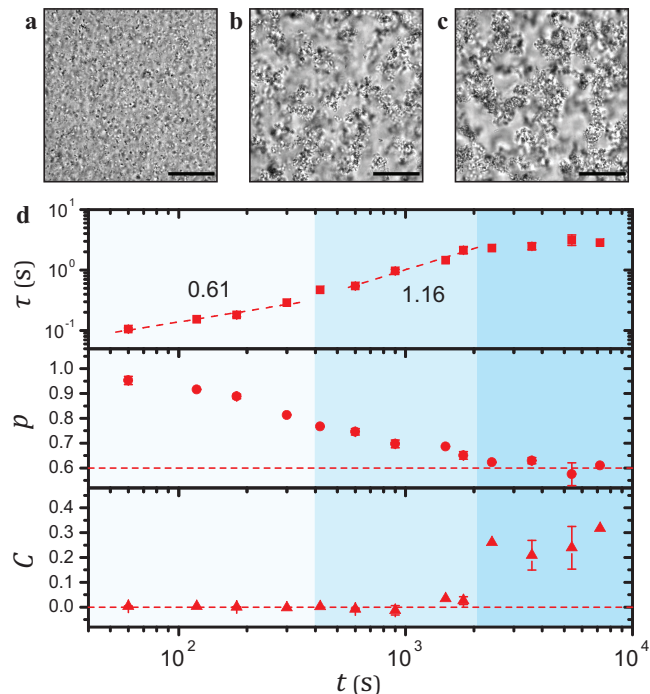


FIG. 1. Micrographs showing the temporal evolution of the gel at particle volume fraction $\phi = 0.8\%$ at times $t = 180$ s (a), 1500 s (b), 7200 s (c) after the onset of aggregation. Scale bars correspond to $30 \mu\text{m}$. (d) Temporal evolution of the relaxation time τ , the stretching exponent p , and the nonergodicity parameter C at a fixed wave vector $q = 4.0 \mu\text{m}^{-1}$ or $qa = 0.47$, where $a = 116.3$ nm is the hydrodynamic radius of a particle.

at half maximum [34]. At all t , p is largely independent of q [29]. Despite these temporal changes in τ and p , the system retains its ergodicity, which implies that the structural rearrangements after the geometric percolation only gradually give rise to rigidity of the network [35, 36].

After the onset of the third stage ($t \approx 2000$ s) shown in Fig. 1(d), the network fluctuations remain partially correlated within the observation time, leading to nonzero values of the nonergodicity parameter $C(q = 4.0 \mu\text{m}^{-1})$. Concurrently, $\tau(q = 4.0 \mu\text{m}^{-1})$ stays nearly constant with t . Yet, complex q -dependence of the dynamics appears upon this transition. For $t < 2000$ s, $C(q) \approx 0$ while $\tau(q) \sim q^{-2.2}$, where the power law exponent is close to -2 of the dilute suspension of monodisperse particles in Brownian motion [32]. For $t > 2000$ s, however, $C(q)$ gradually increases with t while monotonically decreasing with q , as displayed in Fig. 2(a). Simultaneously, $\tau(q)$ flattens, and eventually becomes independent of q for $qa < 0.23$, as displayed in Fig. 2(b). This flattening of $\tau(q)$ marks the end of major temporal evolution, after which all the parameters remain nearly unchanged.

For a more comprehensive inspection of the q -dependence of the dynamics in the aged gels, we employ two objectives ($M = 20\times$ and $60\times$) to extract $\tau(q)$ of the gels at five different ϕ ($= 0.5, 0.8, 1.0, 1.5$ and 2.0%) in their quasi-steady states at sufficiently large t . For each ϕ , three distinct regimes of dynamics emerge, as shown in Fig. 3. In the high- q domain, we observe dynamical hallmarks of fractals. The averaged internal structure of fractal aggregates is fully defined by d_f only, and indeed,

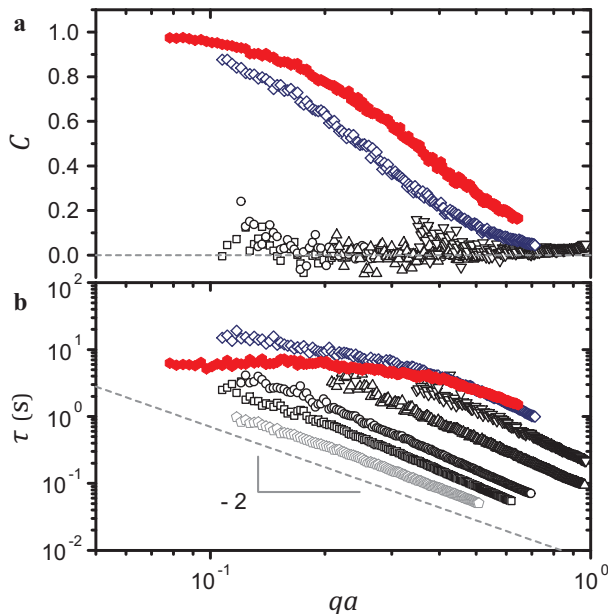


FIG. 2. (a) Nonergodicity parameter C and (b) relaxation time τ of the gel at $\phi = 0.8\%$ as a function of the nondimensionalized wave vector qa at $t = 0$ s (\diamond , stable suspension), 60 s (\square), 180 s (\circ), 600 s (\triangle), 1500 s (∇), 3600 s (\diamond), and 7200 s (closed \circ).

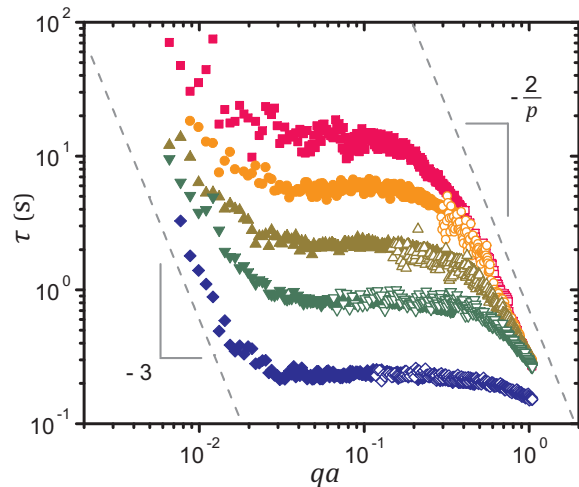


FIG. 3. Relaxation time τ of aged gels in quasi-steady states as a function of the nondimensionalized wave vector qa at $\phi = 0.5\%$ (\square), 0.8% (\circ), 1.0% (\triangle), 1.5% (∇), and 2.0% (\diamond). Closed symbols denote data obtained with a $20\times$ objective and open symbols with a $60\times$ objective.

$\tau(q)$ of all ϕ asymptotically collapse onto a single line, indicating the presence of ϕ -independent structures at the smallest length scales probed. Moreover, according to the model proposed by Reuveni et al. [37, 38], the internal dynamics of a vibrating fractal under thermal perturbation and strong viscous damping for $qR_g \gg 1$, where R_g is the cluster radius of gyration, obeys the following scaling relation in the absence of translational and rotational motion:

$$\tau \sim q^{-2/p}. \quad (2)$$

We obtain $p = 0.66 \pm 0.02$ for all ϕ [29], which yields the value of $-2/p$ consistent with our high- q power law exponent.

In the intermediate- q domain, where τ is independent of q , the motion at the length scale of clusters dominates the gel dynamics. In the model developed by Krall and Weitz for fractal gels [13, 14], $f(q, \Delta t)$ is determined by τ and the maximum mean squared displacement δ^2 at the length scale of the clusters as follows:

$$f(q, \Delta t) = \exp \left[-\frac{q^2 \delta^2}{4} \left(1 - \exp \left[-\left(\frac{\Delta t}{\tau} \right)^p \right] \right) \right], \quad (3)$$

which, for $q^2 \delta^2 \ll 1$, can be simplified to

$$f(q, \Delta t) \approx \frac{q^2 \delta^2}{4} \exp \left[-\left(\frac{\Delta t}{\tau} \right)^p \right] + \left(1 - \frac{q^2 \delta^2}{4} \right), \quad (4)$$

an equivalent functional form to our model in Eq. (1). From Eq. (1) and Eq. (3) in the limit of $\Delta t \rightarrow \infty$,

$$f(q, \Delta t \rightarrow \infty) = \exp \left(-\frac{q^2 \delta^2}{4} \right) = C(q). \quad (5)$$

The resulting δ^2 from curve-fits to $C(q)$ satisfies $q^2 \delta^2 \ll 1$ for the intermediate- q domain [29]. Provided that the

microscopic elasticity of the gels is governed by the local spring constant $\kappa \sim (a/\xi)^\beta$ between two particles of radius a separated by the distance ξ within a fractal cluster, where β is the elasticity exponent [39–41], τ and δ^2 scale with ϕ as

$$\tau \sim \phi^{-\frac{\beta+1}{3-d_f}} \quad (6)$$

and

$$\delta^2 \sim \phi^{-\frac{\beta}{3-d_f}}, \quad (7)$$

respectively [14]. We measure the mean value of the q -independent relaxation time τ_m , and observe the scalings of $\tau_m \sim \phi^{-2.93}$ and $\delta^2 \sim \phi^{-2.07}$, which with $d_f = 1.8$, leads to $\beta = 2.52$ and 2.48 , respectively.

The mean $\beta = 2.50$ reflects considerable structural rearrangements during the network formation. For a percolating chain resistant to bending and stretching, $\kappa \sim N^{-1}R_\perp^{-2}$, where N is the number of particles and R_\perp the radius of gyration of the chain projected onto the plane perpendicular to the line connecting the two ends of the chain [42]. For a chain of end-to-end distance ξ , $N \sim \xi^{d_B}$, where d_B denotes the bond dimension, while $R_\perp \sim \xi^\epsilon$, where ϵ specifies the extent of isotropy of the chain from $\epsilon = 0$ for a perfectly straight chain to $\epsilon = 1$ for an isotropic chain [40]. Consequently, the following scaling relation holds [40, 43]:

$$\kappa \sim \xi^{-(2\epsilon+d_B)} \sim \xi^{-\beta}. \quad (8)$$

The elasticity of a network of fractal aggregates, therefore, is largely conferred by the geometry of the force-bearing backbones. For an ideal network of compactly packed fractal clusters, $\epsilon \approx 1$. Substituting $\beta = 2.50$ and the representative value of $d_B = 1.1$ [44] into Eq. (8), however, we find $\epsilon = 0.70$, implying significant anisotropy of the stress-bearing strands. In Fig. 1(c), we confirm the prevalence of voids present among the fractal clusters, caused by structural rearrangements that deflect the gel backbones to be anisotropic.

We demonstrate that our model simultaneously exhibits the dynamics described in the two models by Reuveni et al. [38] and by Krall and Weitz [14], as it separates the q -dependence of the characteristic relaxation time and that of the nonergodicity into two parameters $\tau(q)$ and $C(q)$, respectively, in Eq. (1). The anomalous diffusion of the subcluster aggregates is ergodic for $qR_g \gg 1$ [38], while the fluctuations at the length scale of the clusters are nonergodic [14]. Yet, the q^2 term in Eq. (3) determines the q -dependence of both the time scale of the decay and the plateau of f as $\Delta t \rightarrow \infty$, by assuming nonergodic processes at all q [14, 29]. In our model, $\tau(q)$ and $C(q)$ allow independent determination of within what time and how far, respectively, scatterers move at each q . We thus suggest that, at the transition between the intermediate- q and the high- q regimes, the

relaxation time of the internal vibrations captured in Eq. (1) simply scales as τ_m , which from Eq. (2) and Eq. (6) leads to

$$q_h \sim \phi^{\frac{p}{2}\left(\frac{\beta+1}{3-d_f}\right)}, \quad (9)$$

where q_h denotes the intermediate-to-high- q transition wave vector. With $p = 0.66$ and $\beta = 2.50$, Eq. (9) yields $q_h \sim \phi^{0.96}$. Using q_h to scale $\tau(q)$ in the abscissa and τ_m in the ordinate, we find that our data of all ϕ collapse onto a mastercurve in the plateau and the high- q domain, as shown in Fig. 4(a).

In the low- q regime, the gels display overdamped dynamics characteristic of a homogeneous viscoelastic medium. The effective spring constant κ between two particles is independent of their distance ξ , if ξ is greater

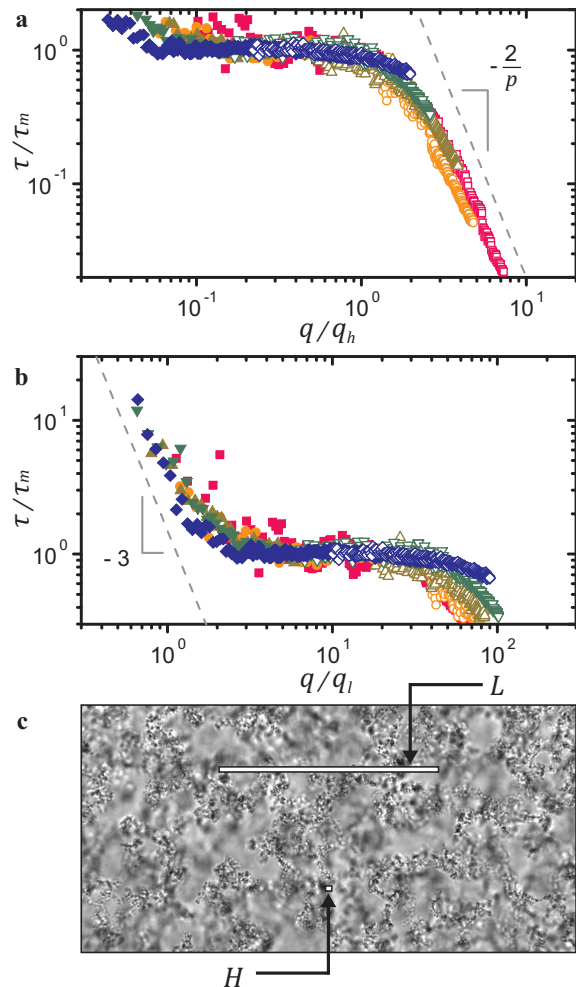


FIG. 4. (a) Relaxation time $\tau(q)$ of all ϕ scaled with the intermediate-to-high- q transition wave vector q_h in the abscissa and the mean τ of the intermediate- q domain τ_m in the ordinate. (b) $\tau(q)$ of all ϕ scaled with the low-to-intermediate- q transition wave vector q_l in the abscissa and τ_m in the ordinate. (c) Micrograph of the aged gel at $\phi = 0.8\%$. Scale bars indicate the length scale of the intermediate-to-high- q transition $H = 2\pi/q_h \approx 3.3 \mu\text{m}$, and the smallest length scale $L = 2\pi/q_l \approx 99.4 \mu\text{m}$, at which $\tau \sim q^{-3}$.

than the smallest length scale L at which the continuum assumption holds true [45], but also sufficiently small such that the effect of the finite system size is negligible. The magnitude of the frictional force that a scatterer experiences in a homogeneous two-phase continuum, however, scales as its volume V [46, 47], as every differential volume undergoes the same amount of viscous coupling between the two phases. Because of the tenuous and porous structure of the network, the total frictional force is expected to be proportional to the number of constituent particles N , which in a continuum scales as $N \sim \phi V$. Thus, in the low- q domain,

$$\tau \sim \frac{\eta a \frac{\phi V}{a^3}}{GL} \sim \frac{\eta \phi q_l}{Ga^2} q^{-3}, \quad (10)$$

where $G \sim \kappa/L$ denotes the bulk shear modulus, with L chosen as the characteristic length scale of the elastic forces and $q_l = 2\pi/L$. Indeed, $\tau(q)$ at $\phi = 2.0\%$ exhibits the scaling of $\tau \sim q^{-3}$ for $qa < 0.012$, as shown in Fig. 3. For Eq. (10) to be valid at all ϕ , we expect $\tau(q) = \psi(\phi)q^{-3}$, where $\psi(\phi) \sim \tau_m(\phi)q_l(\phi)^3$. Because τ_m denotes the time scale of the floppiest mode of the gel network, it also sets G by

$$G = \frac{6\pi\eta b_m}{\tau_m}, \quad (11)$$

where b_m is a correction factor [14]. Substituting the general form of $\tau(q)$ into Eq. (10) and using $\tau_m(\phi) \sim G(\phi)^{-1}$ from Eq. (11), therefore, results in

$$q_l \sim \phi^{0.5}. \quad (12)$$

Given that $q_l a \approx 0.012$ marks the upper bound of the power law behavior $\tau \sim q^{-3}$ for $\phi = 2.0\%$, as displayed in Fig. 3, scaling $\tau(q)$ of all ϕ with the corresponding values of q_l in the abscissa and τ_m in the ordinate leads to a mastercurve in the low- q and the intermediate- q domains, as shown in Fig. 4(b). The scaling in Eq. (12) differs from that of the DLCA cluster radius $R_c^{-1} \sim \phi^{1/(3-d_f)} = \phi^{0.8}$ [39], since the bulk elasticity, as well as the structure, governs the dynamical length scale L . For visual inspection, we insert a scale bar of length L in the micrograph of the gel at $\phi = 0.8\%$ in Fig. 4(c). We also include a scale bar that corresponds to the intermediate-to-high- q transition $H = 2\pi/q_h$ to highlight the contrast between the length scales of the low- q and the high- q regimes.

The direct link between τ and G indicates that we can estimate the macroscopic shear modulus G of the gels by measuring the microscopic relaxation time τ in either the intermediate- q domain or, as long as we can identify q_l , the low- q domain. Using Eq. (11) with $b_m = 2.7$, we observe that the resulting values of G yield a smooth continuation of the storage modulus G' obtained from conventional rheometry, as shown in Fig. 5. Alternatively, G can be estimated by measuring ψ and q_l from

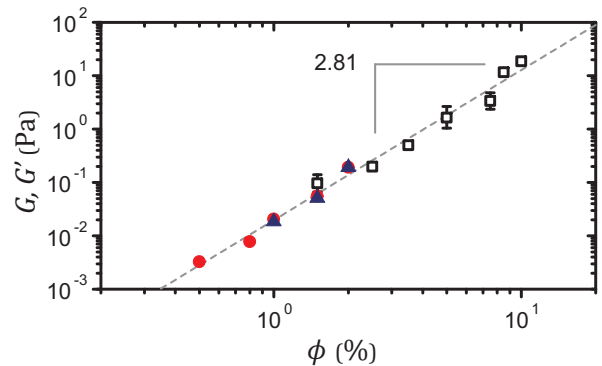


FIG. 5. Storage modulus G' (\square) obtained from conventional rheometry and shear modulus G estimated from DDM in the intermediate- q domain (closed \circ) and the low- q domain (closed \triangle). The DDM estimates show consistent power laws.

Fig. 3, if the power law behavior of $\tau \sim q^{-3}$ is accessible. The following rearranged form of Eq. (10)

$$G = \frac{\eta \phi q_l b_l}{a^2 \psi}, \quad (13)$$

where $b_l = 1.2$ is a correction factor, yields consistent scaling behavior of G , as displayed in Fig. 5.

Our dynamical investigation of evolving colloidal gels unveils the extensive kinetic route through particle aggregation, geometric percolation, and emergence of non-ergodicity that establishes distinct dynamical regimes at different length scales. In particular, we show that internal vibrations of random fractals, cluster-dominated fluctuations, and homogeneity of a viscoelastic medium simultaneously define the nonergodic colloidal gels. Consequently, our results not only demonstrate links among different models, but clarify their limits. We expect a similar application of DDM to other soft materials can likewise provide comprehensive descriptions of their multiscale dynamics [48].

We thank Veronique Trappe and Fabio Giavazzi for helpful discussions. J.H.C. and I.B. acknowledge support from the Research Support Committee and Kwanjeong Educational Foundation. R.C. acknowledges support from Regione Lombardia and CARIPLO Foundation, Grant No. 2016-0998.

-
- [1] P. Meakin, Phys. Rev. Lett. **51**, 1119 (1983).
 - [2] D. A. Weitz and M. Oliveria, Phys. Rev. Lett. **52**, 1433 (1984).
 - [3] M. Y. Lin, H. M. Lindsay, D. A. Weitz, R. C. Ball, R. Klein, and P. Meakin, Phys. Rev. A **41**, 2005 (1990).
 - [4] M. Carpineti and M. Giglio, Phys. Rev. Lett. **68**, 3327 (1992).
 - [5] P. J. Lu, E. Zaccarelli, F. Ciulla, A. B. Schofield, F. Sciortino, and D. A. Weitz, Nature **453**, 499 (2008).
 - [6] E. Zaccarelli, J. Phys. Condens. Matter **19**, 323101 (2007).

- [7] R. N. Zia, B. J. Landrum, and W. B. Russel, *J. Rheol.* **58**, 1121 (2014).
- [8] Y. Gao, J. Kim, and M. E. Helgeson, *Soft Matter* **11**, 6360 (2015).
- [9] L. Cipelletti, S. Manley, R. C. Ball, and D. A. Weitz, *Phys. Rev. Lett.* **84**, 2275 (2000).
- [10] S. Manley, B. Davidovitch, N. R. Davies, L. Cipelletti, A. E. Bailey, R. J. Christianson, U. Gasser, V. Prasad, P. N. Segrè, and M. P. Doherty *et al.*, *Phys. Rev. Lett.* **95**, 048302 (2005).
- [11] J. M. van Doorn, J. Bronkhorst, R. Higler, T. van de Laar, and J. Sprakel, *Phys. Rev. Lett.* **118**, 188001 (2017).
- [12] M. Bouzid, J. Colombo, L. V. Barbosa, and E. Del Gado, *Nat. Commun.* **8**, 15846 (2017).
- [13] A. H. Krall, Z. Huang, and D. A. Weitz, *Physica A* **235**, 19 (1997).
- [14] A. H. Krall and D. A. Weitz, *Phys. Rev. Lett.* **80**, 778 (1998).
- [15] P. N. Segrè, V. Prasad, A. B. Schofield, and D. A. Weitz, *Phys. Rev. Lett.* **86**, 6042 (2001).
- [16] S. Manley, H. M. Wyss, K. Miyazaki, J. C. Conrad, V. Trappe, L. J. Kaufman, D. R. Reichman, and D. A. Weitz, *Phys. Rev. Lett.* **95**, 238302 (2005).
- [17] M. Laurati, G. Petekidis, N. Koumakis, F. Cardinaux, A. B. Schofield, J. M. Brader, M. Fuchs, and S. U. Egelhaaf, *J. Chem. Phys.* **130**, 134907 (2009).
- [18] S. Romer, F. Scheffold, and P. Schurtenberger, *Phys. Rev. Lett.* **85**, 4980 (2000).
- [19] F. Scheffold, S. E. Skipetrov, S. Romer, and P. Schurtenberger, *Phys. Rev. E* **63**, 061404 (2001).
- [20] H. M. Wyss, S. Romer, F. Scheffold, P. Schurtenberger, and L. J. Gauckler, *J. Colloid Interface Sci.* **241**, 89 (2001).
- [21] J. Liu, V. Boyko, Z. Yi, and Y. Men, *Langmuir* **29**, 14044 (2013).
- [22] D. C. E. Calzolari, I. Bischofberger, F. Nazzani, and V. Trappe, *J. Rheol.* **61**, 817 (2017).
- [23] H. Guo, S. Ramakrishnan, J. L. Harden, and R. L. Leheny, *J. Chem. Phys.* **135**, 154903 (2011).
- [24] Q. Zhang, D. Bahadur, E. M. Dufresne, P. Grybos, P. Kmon, R. L. Leheny, P. Maj, S. Narayanan, R. Szczygiel, S. Ramakrishnan, and A. Sandy, *Phys. Rev. Lett.* **119**, 178006 (2017).
- [25] R. Cerbino and V. Trappe, *Phys. Rev. Lett.* **100**, 188102 (2008).
- [26] F. Giavazzi, D. Brogioli, V. Trappe, T. Bellini, and R. Cerbino, *Phys. Rev. E* **80**, 031403 (2009).
- [27] F. Giavazzi and R. Cerbino, *J. Opt.* **16**, 083001 (2014).
- [28] N. Dingenouts, C. Norhausen, and M. Ballauff, *Macromolecules* **31**, 8912 (1998).
- [29] See Supplemental Material for the synthesis protocol of the PS-PNIPAM particles, the curve-fitting methods, and more details of our DDM analysis.
- [30] D. A. Weitz, J. S. Huang, M. Y. Lin, and J. Sung, *Phys. Rev. Lett.* **53**, 1657 (1984).
- [31] P. G. J. van Dongen and M. H. Ernst, *Phys. Rev. Lett.* **54** (1985).
- [32] P. N. Pusey, in *Neutrons, X-rays and Light Scattering Methods Applied to Soft Condensed Matter*, edited by P. Lindner and T. Zemb (Elsevier, Amsterdam, 2002) 1st ed., Chap. 9.
- [33] P. J. Lu, F. Giavazzi, T. E. Angelini, E. Zaccarelli, F. Jargstorff, A. B. Schofield, J. N. Wilking, M. B. Romanowsky, D. A. Weitz, and R. Cerbino, *Phys. Rev. Lett.* **108**, 218103 (2012).
- [34] D. C. Johnston, *Phys. Rev. B* **74**, 184430 (2006).
- [35] H. Tsurusawa, M. Leocmach, J. Russo, and H. Tanaka, *Sci. Adv.* **5**, 6090 (2019).
- [36] S. Zhang, L. Zhang, M. Bouzid, D. Z. Rocklin, E. Del Gado, and X. Mao, *Phys. Rev. Lett.* **123**, 058001 (2019).
- [37] S. Reuveni, J. Klafter, and R. Granek, *Phys. Rev. Lett.* **108**, 068101 (2012).
- [38] S. Reuveni, J. Klafter, and R. Granek, *Phys. Rev. E* **85**, 011906 (2012).
- [39] W. H. Shih, W. Y. Shih, S. I. Kim, J. Liu, and I. A. Aksay, *Phys. Rev. A* **42**, 4772 (1990).
- [40] R. de Rooij, D. van den Ende, M. H. G. Duits, and J. Mellema, *Phys. Rev. E* **49**, 3038 (1994).
- [41] A. H. L. West, J. R. Melrose, and R. C. Ball, *Phys. Rev. E* **49**, 4237 (1994).
- [42] Y. Kantor and I. Webman, *Phys. Rev. Lett.* **52**, 1891 (1984).
- [43] S. Romer, H. Bissig, P. Schurtenberger, and F. Scheffold, *Europhys. Lett.* **108**, 48006 (2014).
- [44] P. Meakin, I. Majid, S. Havlin, and H. E. Stanley, *J. Phys. A* **17**, L975 (1984).
- [45] A. D. Dinsmore, V. Prasad, I. Y. Wong, and D. A. Weitz, *Phys. Rev. Lett.* **96**, 185502 (2006).
- [46] A. J. Levine and T. C. Lubensky, *Phys. Rev. Lett.* **85**, 1774 (2000).
- [47] A. J. Levine and T. C. Lubensky, *Phys. Rev. E* **63**, 041510 (2001).
- [48] R. Cerbino and P. Cicuta, *J. Chem. Phys.* **147**, 110901 (2017).